$$1/2O_{2(g)} + 2YBa_2Cu_3O_{7(s)} = Y_2O_{3(s)} + 2Ba_2Cu_3O_{6(s)} \quad (2)$$

The enthalpy of this decomposition reaction is -130 ± 24 kJ/mol. As in the decomposition of $YBa_2Cu_4O_8$, the decomposition reaction of $YBa_2Cu_3O_7$, with respect to $Ba_2Cu_3O_6$ and Y_2O_3, involves the transfer of a half mole of gaseous oxygen to the lattice, with an entropic $-T\Delta S_{rx}$ contribution of approximately +30 kJ/mol. We compared the free energies of decomposition of both $YBa_2Cu_4O_8$ and $YBa_2Cu_3O_{7-x}$ with respect to $Ba_2Cu_3O_6$; our comparison reaffirms that $YBa_2Cu_4O_8$ is more stable at low temperatures than $YBa_2Cu_3O_{7-x}$.

As expected, the phase relations in this system appear to be controlled by the oxidation thermodynamics of the copper ion; as the temperature of the system is reduced, higher formal valence states for copper are stabilized in electropositive lattice environments (*8*, *20*). For the perovskite-related cuprates, the oxidation of copper from a formal valence of 2^+ to 3^+ is exothermic, releasing ~200 kJ per mole of O_2 (*12*, *21*, *22*); this favorable contribution to the partial molar ΔG_{rx} is, of course, balanced by the decrease in entropy of the system from the transformation of oxygen from the gaseous state to the solid state.

In this Y-Ba-Cu-O system, the highest formal valence occurs in the binary compound $Ba_2Cu_3O_6$; the average copper valence in this compound is +2.66 compared to +2.33 in $YBa_2Cu_3O_7$. A complete understanding of why $Ba_2Cu_3O_6$ exhibits such high stability at low temperatures, and thus why the superconductors are metastable, will require knowledge of the $Ba_2Cu_3O_6$ structure (it has not been completely refined). Previous electron and x-ray diffraction studies (*17*, *18*) suggest that the structure is closely related to that of the trivalent cuprate, $NaCuO_2$. This structure, in which infinite one-dimensional chains of edge-shared cuprate groups are linked by the larger electropositive cations, is adopted by several highly oxidized cuprates. For example, closely related $ACuO_2$ phases can be stabilized at low temperatures for A = K (*23*), Cs (*24*), and Rb (*25*). The same arrangement of cuprate chains is also found in the low-temperature form of calcium cuprate, $Ca_{1-x}CuO_2$ (x = 0.8 to 0.85) (*26*) and in several ternary calcium–rare earth (RE) compounds, such as $(Ca_{2-x}RE_{2+x})Cu_5O_{10}$ (RE = Y, Gd, Nd) (*27*). The reduced occupancy of the larger interchain cation sites in these cation-deficient compounds is accommodated by a modulation of the positions of the larger cations. It is these modulations, which can be commensurate or incommensurate, that have complicated the refinements of these compounds. However, the published models for $Ba_2Cu_3O_6$, or $Ba_{0.67}CuO_2$, indicate that this may be another example of a stable modulated $NaCuO_2$-type structure. Apparently the higher electropositive environment provided by this structure is particularly effective in increasing the stability of the trivalent state for copper.

REFERENCES AND NOTES

1. T. H. Geballe, *Mater. Res. Sre. Bull.* **17**, 70 (July 1992).
2. C. T. Lynch, Ed., *Handbook of Materials Science* (CRC Press, Cleveland, OH, 1975), pp. 106–114.
3. T. Egami *et al.*, in *High-Temperature Superconductivity: Physical Properties, Microscopic Theory, and Mechanisms*, J. Ashkenazi, S. Barnes, F. Zuo, G. Vezzoli, B. Klein, Eds. (Plenum, New York, 1991), pp. 389–399.
4. B. H. Toby, T. Egami, J. D. Jorgensen, M. A. Subramanian, *Phys. Rev. Lett.* **64**, 2414 (1990).
5. J. Mustre de Leon, S. D. Conradson, I. Batistic, A. R. Bishop, *ibid.* **65**, 1675 (1990).
6. J. Mustre de Leon, I. Batistic, A. R. Bishop, S. D. Conradson, S. A. Trugman, *ibid.* **68**, 3236 (1992).
7. A. W. Sleight, *Phys. Today* **44**, 24 (June 1991).
8. ———, *Physica C* **162–164**, 3 (1989).
9. J. C. Phillips, *Physics of High-T_c Superconductors* (Academic Press, New York, 1989).
10. L. R. Morss, S. E. Dorris, T. B. Lindemer, N. Naito, *Eur. J. Solid State Inorg. Chem.* **27**, 327 (1990).
11. F. H. Garzon, I. D. Raistrick, D. S. Ginley, J. W. Halloran, *J. Mater. Res.* **6**, 885 (1991).
12. F. H. Garzon and I. D. Raistrick, in *Proceedings of the International Conference on the Chemistry of Electronic Ceramic Materials*, P. Davies and R. Roth, Eds. (NIST Spec. Publ. 804, National Institute of Standards and Technology, Gaithersburg, MD, 1990), p. 373.
13. Z. Zhou and A. Navrotsky, *J. Mater. Res.* **7**, 2920 (1992).
14. A. Navrotsky, in *Proceedings of the International Conference on the Chemistry of Electronic Ceramic Materials*, P. Davies and R. Roth, Eds. (NIST Spec. Publ. 804, National Institute of Standards and Technology, Gaithersburg, MD, 1990), p. 379.
15. E. L. Brosha *et al.*, *Physica C* **184**, 353 (1991).
16. R. Beyers and B. T. Ahn, *Annu. Rev. Mater. Sci.* **21**, 335 (1991).
17. J. G. Thompson, J. D. Fitz Gerald, R. L. Withers, P. J. Barlow, J. S. Anderson, *Mater. Res. Bull.* **24**, 505 (1989).
18. J. G. Thompson *et al.*, *Mater. Forum* **14**, 27 (1990).
19. O. Kubaschewski and C. B. Alcock, *Metallurgical Thermodynamics* (Pergamon, Oxford, ed. 5, 1979), p. 282.
20. J. Gopalakrishnan, M. A. Subramanian, A. W. Sleight, *J. Solid State Chem.* **80**, 156 (1989).
21. E. Thiele and P. K. Davies, *J. Am. Ceram. Soc.* **74**, 1011 (1991).
22. M. E. Parks *et al.*, *J. Solid State Chem.* **79**, 53 (1989).
23. N. E. Brese, M. O'Keeffe, R. B. Von Dreele, V. G. Young, *ibid.* **83**, 1 (1989).
24. K. Wahl and W. Klemm, *Z. Anorg. Allg. Chem.* **270**, 69 (1952).
25. H. D. Wasel-Nielen and R. Hoppe, *ibid.* **375**, 43 (1970).
26. T. Siegrist, R. S. Roth, C. J. Rawn, J. J. Ritter, *Chem. Matters.* **2**, 192 (1990).
27. P. K. Davies, *J. Solid State Chem.* **95**, 365 (1991).
28. L. R. Morss, D. C. Sonnenberger, R. J. Thorn, *Inorg. Chem.* **27**, 2106 (1988).

29. Supported in part by a grant from the NSF (DMR-92-00800) and from ITT Defense, GE Aerospace, and the Commonwealth of Pennsylvania through the Ben Franklin Superconductivity Center.

16 November 1992; accepted 4 February 1993

Electrostatic Screening of Charge and Dipole Interactions with the Helix Backbone

David J. Lockhart and Peter S. Kim

Electrostatic interactions in proteins are potentially quite strong, but these interactions are mitigated by the screening effects of water, ions, and nearby protein atoms. The early work of Kirkwood and Westheimer on small organic molecules showed that the extent of the screening may depend on whether charged or dipolar groups are involved. The dielectric and ionic screening of the interactions between the dipolar backbone amide groups of monomeric α helices and either (i) solvent-exposed charges or (ii) solvent-exposed dipoles at the amino terminus was measured. The dielectric screening effects are an order of magnitude greater for the backbone-charge interactions than for the backbone-dipole interactions, and the ionic strength dependence is substantially different in the two cases. These results suggest that interactions that involve the dipolar groups of proteins may be relatively more important for stability and function than is generally thought.

The screening of electrostatic interactions results primarily from electronic polarization, reorientation of dipolar groups, and changes in the concentrations of charged species in the vicinity of charges and dipoles. These effects are well understood and can be accurately determined for interactions in isotropic, homogeneous media. However, in complex inhomogeneous environments such as those near the surface of proteins, dielectric and ionic screening is difficult to predict. In these cases, factors such as the shape and composition of the surface and whether the interactions involve charged or dipolar groups are expected to be especially important. Structurally well defined peptides provide good model systems in which to study screening effects on electrostatic interactions at protein surfaces.

We have measured previously the interaction between the backbone of short, stable monomeric α helices and a solvent-exposed

Howard Hughes Medical Institute, Whitehead Institute for Biomedical Research, Department of Biology, Massachusetts Institute of Technology, 9 Cambridge Center, Cambridge, MA 02142.

dipolar group through an internal Stark effect measurement of the electric field at the NH_2-terminus (*1*, *2*). The magnitude of the electric field is proportional to the strength of the backbone-dipole interaction. Here, we determined the strength of the electrostatic interaction between NH_2-terminal charges and the same set of helices, from the shift in the pK_a (K_a, acid dissociation constant) of titratable groups in the presence of helical structure. The pK_a shift is linked thermodynamically to the effect of the charge on the free energy of helix formation and, in the absence of side chain interactions and structural relaxation, is proportional to the backbone-charge interaction energy. In order to study ionic screening effects, we made the two types of measurements at several ionic strengths.

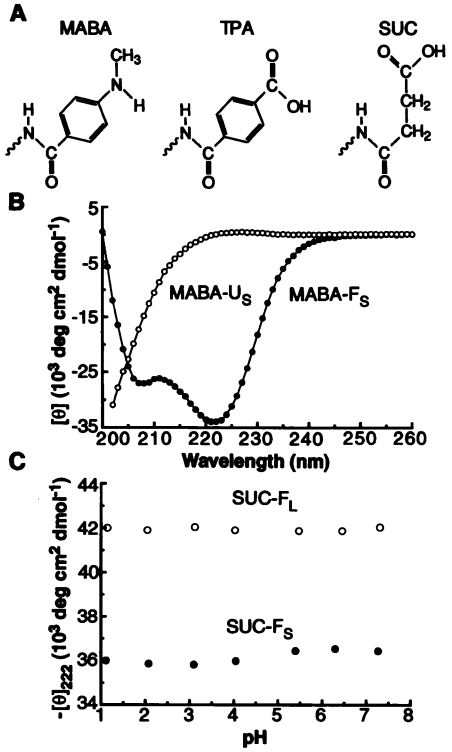

Fig. 1. NH_2-terminal titratable groups (NTGs) and CD data for peptides with titratable groups attached. (**A**) Structures of the neutral forms of the NTGs, including the amide link to the NH_2-terminus of the peptide. The carbonyl oxygen of this amide bond can act as a hydrogen-bond acceptor for the amide proton of residue 4, stabilizing the end of the helix and, for MABA and TPA, defining the position of the charge relative to the backbone. (**B**) CD spectra of peptides F_S and U_S with neutral MABA attached (pH 7, 0°C). The CD spectra of these peptides with the other NTGs attached and the spectra of the other F and U peptides with the various NTGs attached are similar. (**C**) Peptide structure for both the 21- and 41-residue helices is largely unaffected by titration of the SUC group. The pH dependence of $[\theta]_{222}$ (0°C) for peptides F_S and F_L with SUC attached is shown. The magnitude of $[\theta]_{222}$ for F_L is expected to be greater than for F_S because of the dependence of the CD signal on helix length (*30*). However, the absolute values of $[\theta]_{222}$ are accurate only to approximately ±10% because of uncertainty in the concentration determination by quantitative amino acid analysis.

Three different NH_2-terminal titratable groups (NTGs) were used: 4-methylaminobenzoyl (MABA), 4-carboxybenzoyl [terephthalate (TPA)], and succinylic acid (SUC) moieties. The NTGs are attached covalently to the NH_2-terminus through an amide linkage (Fig. 1A). The carbonyl oxygen of the amide bond between the NTGs and the peptide can hydrogen-bond to the amide proton of residue 4. For MABA and TPA, this hydrogen bond defines the position of the group, except for a ring flip that does not change the location of the charge. The charge on the SUC group can be closer to the helix backbone, but the position is not defined exactly because of rotational freedom about the C–C single bonds.

The peptides used were (*3*)

F_S: -AAAAA(AAARA)$_3$A-CONH$_2$
F_L: -AAAAA(AAARA)$_7$A-CONH$_2$
U_S: -AAPAA(APARA)$_3$A-CONH$_2$

F_SR5: -(AAAAR)$_4$A-CONH$_2$
U_SR5: -(AAPAR)$_4$A-CONH$_2$

F_LR5: -(AAAAR)$_8$A-CONH$_2$
U_LR5: -(AAPAR)$_8$A-CONH$_2$

where A is Ala, R is Arg, and P is Pro; F and U indicate peptides designed to be folded or unfolded, respectively; subscripts S and L denote short peptides and their longer versions, respectively; and R5 denotes the presence of an Arg residue at position 5. There are no residues in these peptides that titrate between pH 1 and 8.

Table 1. Observed pK_a shifts, free-energy changes, and melting temperatures (T_m) for the helical peptides with different NH_2-terminal groups. The peptide melting temperature was measured by the CD signal at 222 nm at a pH where the NTG is uncharged (*4*). Values for ΔpK_a, the change in pK_a of the NTG in the presence of helical structure, are relative to the appropriate unfolded control (*7–9*). The change in the free energy of helix formation ($\Delta\Delta G$; kcal/mol) is the value for the charged form of the NTG minus the value for the neutral form. A negative value for $\Delta\Delta G$ indicates that the helix is stabilized by the charge on the titratable group.

Peptide	NTG	T_m (°C)	Charge	ΔpK_a	$\Delta\Delta G$
F_S	MABA	35	(+)	−0.45	+0.57
	TPA	34	(−)	−0.28	−0.35
	SUC	39	(−)	−0.55	−0.70
F_L	MABA	52	(+)	−0.51	+0.64
	SUC	54	(−)	−0.52	−0.66
F_SR5	MABA	33	(+)	−0.49	+0.62
F_LR5	MABA	50	(+)	−0.57	+0.72

The rationale for the design of these peptides and the measurement of their properties have been discussed previously (*1*).

Circular dichroism (CD) measurements (Fig. 1B) indicate that with the NTGs attached, the F peptides are highly helical (at both low and high pH), monomeric (*4*), soluble in water (>4 mM), and quite stable (Table 1). Two-dimensional nuclear magnetic resonance (2D-NMR) experiments on peptide F_S with the NTGs attached (*5*) (Table 2) suggest that the NH_2-termini are not frayed significantly. Furthermore, the relative strengths of the nuclear Overhauser effect (NOE) crosspeaks between the α proton of Ala^1 (H^{α}_1) and the amide and β protons of Ala^4 (H^{N}_4 and H^{β}_4, respectively) are consistent with α-helical, not 3_{10}-helical, structure (*6*).

The unfolded U_S and U_L peptides also contain Ala at positions 1 and 2 near the probe but contain several prolines that disrupt helical structure (Fig. 1B). These unfolded control molecules allow the properties of the attached probes to be measured in the absence of helical structure but under otherwise identical conditions. The control molecules permit pK_a shifts to be determined without the need to make corrections for the effects of chemical denaturants or temperature or to assume a generic, unperturbed pK_a value in the unfolded state.

Table 2. Volume integrals for NH_2-terminal NOESY crosspeaks in peptide F_S with MABA or TPA attached (*5*). We collected data at pH values where MABA and TPA are either neutral (O) or charged (+ or −) to check for structural changes upon titration. The 2D-NMR spectrum of peptide F_S with neutral MABA has been shown previously (*1*). To facilitate comparison of NOE intensities, we normalized the volume integrals for each sample by using the sum of the intraresidue NOEs listed at the bottom. All 2D-NMR spectra were recorded and processed identically (*5*).

NOE	MABA		TPA	
	pH 1.2 (+)	pH 5.6 (O)	pH 2 (O)	pH 5.7 (−)
	Interresidue			
H^{N}_1–H^{N}_2	26	25	24	~21*
H^{N}_2–H^{N}_3	39	41	50	44
H^{N}_3–H^{N}_4	>20*	>19*	43	>27*
H^{α}_1–H^{N}_4	7	8	6	7
H^{α}_1–H^{β}_4	59	−†	~52*	~58*
H^{N}_2–H^{α}_1	21	−†	18	14
H^{N}_2–H^{β}_1	38	39	41	42
	Intraresidue			
H^{N}_1–H^{α}_1	51	52	48	48
H^{N}_2–H^{α}_2	57	52	51	49
H^{N}_1–H^{β}_1	90	94	95	103
H^{N}_2–H^{β}_2	101	100	107	102

*NOE crosspeak volumes can only be estimated because of proximity to the diagonal or a small amount of overlap with other crosspeaks. †Overlap with other crosspeaks prevents reliable integration.

In order for the pK_a shifts to be interpretable in terms of electrostatic interactions, structural changes upon titration must be minimal. Titration of SUC leads to only slight changes in the CD signal at 222 nm for helical peptides F_S and F_L (Fig. 1C). Moreover, the NH_2-terminal NOE cross-peak intensities for peptide F_S are largely unchanged upon protonation or deprotonation of either MABA or TPA (Table 2).

The pH titrations of MABA attached to F_S, F_L, and U_S and the corresponding fits to the equation for a single ionization equilibrium are shown in Fig. 2A (*7*). The pK_a shifts are summarized in Table 1 (*8*). The shift in the pK_a of the conjugate acid of MABA in the presence of helical structure is 0.45 ± 0.03 pH units for peptide F_S. The pK_a shift is only slightly larger in the presence of a positively charged Arg side chain at position 5 (peptide F_SR5), which indicates that the shift is the result of interactions between the NH_2-terminal charge and the helix backbone, not side chain charges. The pK_a shifts for MABA attached to the longer, 41-residue peptides F_L and F_LR5 are larger by only 9% and 16%, respectively, compared with the shorter counterparts.

Whereas titration of MABA introduces a positive charge, a negative charge is placed near the NH_2-terminus by deprotonation of either TPA or SUC. The pK_a of TPA is shifted by 0.28 pH units for peptide F_S in the presence of helical structure at 0°C. For SUC, a larger shift is expected because the negative charge of the carboxylate can be considerably closer to the backbone groups in the first turn of the helix. The pK_a shift for SUC is ~0.5 pH units, and the data for the 21- and 41-residue helices are nearly superimposable (Fig. 2B) (*9*).

The backbone-charge interaction energy decreases rapidly with increasing ionic strength (Fig. 3A). The magnitude of the pK_a shift for MABA (attached to peptide F_S) decreases roughly exponentially with the square root of the monovalent salt concentration and is reduced to one-half the initial value in ~250 mM NaCl. Similar ionic screening effects have been observed by others (*10–12*). In contrast, the backbone-dipole interactions are much less sensitive to the presence of ions (*1*); ~3 M NaCl is required for a twofold reduction in the magnitude of the backbone-dipole interaction (Fig. 3A).

The change in pK_a of the titratable groups is related to the effect of the charge on the free energy of helix formation, $\Delta\Delta G_F$, by the equation [see, for example, (*13, 14*)]

$$\Delta\Delta G_F = 2.3RT\Delta pK_a \quad (1)$$

where $\Delta\Delta G_F$ is the difference in the free energy of helix formation (basic form of the NTG minus the acidic form), R is the gas constant, T is temperature, and ΔpK_a is the pK_a shift in the presence of helical structure (helical minus unfolded) (Table 1). As observed previously, NH_2-terminal negative charges stabilize the helices, whereas positive charges are destabilizing (*11, 12, 14, 15*). The absence of an increase in the pK_a shifts with longer helices is consistent with our previous measurement of the electric field at the NH_2-terminus (*1*), simple electrostatic considerations (*16*), and the results of recent theoretical calculations (*17*).

The net screening effects of the environment can be estimated by comparing the experimental interaction energies with the values expected from simple electrostatics. A quantity called the effective dielectric constant, ε_{eff}, is defined as the ratio of the backbone-charge interaction, calculated with Coulomb's law (*18*) and a dielectric constant of 1 (as if there is no environment), to the experimentally determined values (*1, 13, 19, 20*). From the MABA data, ε_{eff} is calculated to be ~40, and from the TPA and SUC data the effective dielectric constant is calculated to be 70 and 95 (*21*), respectively (the dielectric constant of bulk water is 88 at 0°C). The value of 40 calculated from the MABA data is a lower limit because of an additional electronic contribution to the pK_a shift (*22*). In contrast, backbone-dipole interactions in the same helical peptides (with neutral MABA as the dipolar probe) are much less effectively screened (*1*), with an effective dielectric constant at low ionic strength of ~8. A difference in dielectric screening effects in aqueous solution has also been observed previously for organic acids with either charged or dipolar substituents (*13, 23, 24*).

Coulomb's law predicts, given a uniform dielectric constant, that the electrostatic interaction of the backbone with a charge near the NH_2-terminus will be considerably stronger than the interaction with a similarly located dipolar group. However, because backbone-dipole interactions are screened to a lesser extent, they can be comparable in magnitude to or even stronger than backbone-charge interactions, depending on the ionic strength of the solution (*25*). For example, the energy of the interaction between the helix backbone and an NH_2-terminal charge at low ionic

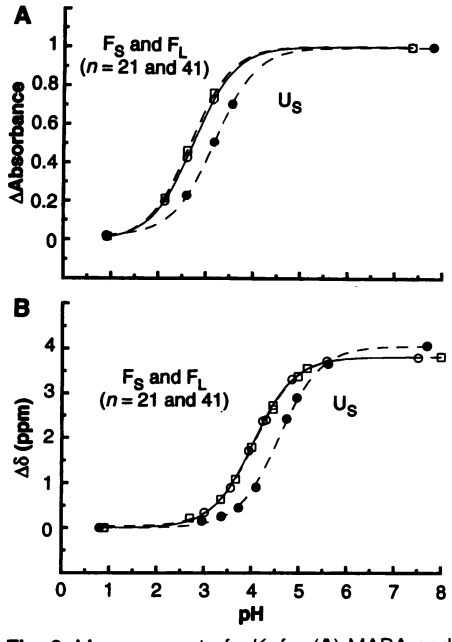

Fig. 2. Measurement of pK_a for (**A**) MABA and (**B**) SUC attached to peptides F_L (□), F_S (○), and U_S (●) at 0°C. The lines are fits to a single ionization equilibrium. In (A), the pK_a value of the conjugate acid of MABA is shifted to a lower pH by 0.45 and 0.52 pH units in the presence of the 21- and 41-residue helical peptides F_S and F_L, respectively. In (B), the pK_a of SUC is shifted by 0.55 and 0.52 pH units for peptides F_S and F_L, respectively. Titration of MABA is determined from the change in absorbance at 297 nm (F peptides) or 292 nm (U peptides) (*8*). The pK_a of SUC is determined from the pH dependence of the chemical shift of the carboxyl carbon labeled specifically with ^{13}C (*9*).

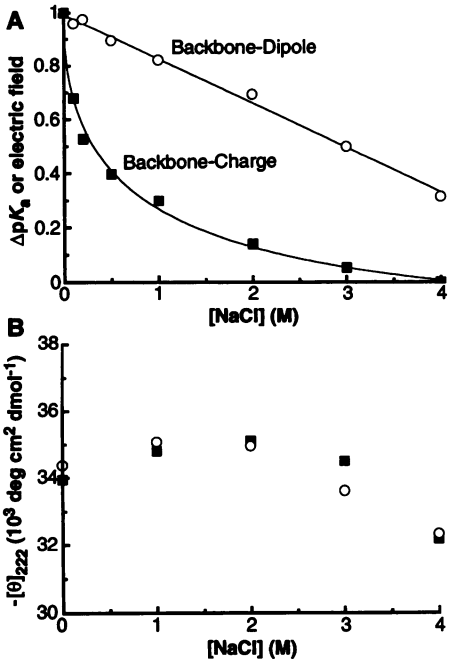

Fig. 3. Dependence of the electrostatic interactions and peptide structure on the concentration of NaCl. (**A**) NaCl dependence of the backbone-charge (pK_a shift) and the backbone-dipole [NH_2-terminal electric field; (*1*)] interactions. (**B**) NaCl dependence of $[\theta]_{222}$ for peptide F_S with MABA attached at pH 1 (○) and pH 7 (■) (note the expanded scale). In (A), the pK_a shift and the electric field data are normalized to an initial value of 1.0 to facilitate comparison. The solid lines are intended as guides. The data in (B) indicate that peptide structure is largely unaffected by increasing NaCl concentration (up to 4 M) at either pH.

strength is as large as 0.7 kcal/mol (Table 1). This value is similar, given the NH_2-terminal electric field measured previously for the same helical peptides (*1*), to the energy of the interaction between the helix backbone and an amide group (with a dipole moment of ~3.5 D). Moreover, at physiological ionic strengths (~200 mM) the backbone-charge interactions are reduced even further, whereas the backbone-dipole interactions are largely unaffected (Fig. 3A).

Qualitatively, differential screening effects can be understood in terms of simple continuum models that take the size and geometry of the interacting groups into consideration (*12, 13, 20, 23, 26*). The physical picture in these models is that the interacting charged and dipolar groups occupy a single low-dielectric region that is surrounded by a high-dielectric continuum that can screen the interactions. The ions and high-dielectric solvent of the continuum are excluded sterically from the immediate vicinity of the interacting groups by a short distance, and the electrostatic response of the continuum is reduced by this separation. As pointed out previously by Gilson *et al.* (*20*), because electrostatic interactions with dipoles decrease more rapidly with distance than interactions with charges (*27*), the response of the continuum and, hence, the screening effects are predicted to be smaller in the case of dipoles (*28*). In addition, there may be contributions to the screening that result from specific interactions between water, ions, and surface groups (*13, 20, 24, 29*).

As predicted by Kirkwood and Westheimer (*13*), different types of intramolecular electrostatic interactions may not be affected equally by the dielectric and ionic environment. The extent of the differences in screening at protein surfaces, however, cannot be predicted accurately on the basis of the earlier small molecule studies because screening is expected to depend on molecular size and geometry and on the locations of the interacting groups. Our results indicate that at the surface of an α helix, the screening effects are quite different for interactions of the backbone with either charges or dipoles. More generally, these results suggest that interactions between dipolar groups such as the backbone amides may be relatively more important for the properties of proteins than is generally thought.

REFERENCES AND NOTES

1. D. J. Lockhart and P. S. Kim, *Science* **257**, 947 (1992).
2. A shift in a charge-transfer absorption band of heme in response to a nearby charged group in myoglobin has also been interpreted to result from an internal Stark effect [R. Varadarajan, D. G. Lambright, S. G. Boxer, *Biochemistry* **28**, 3771 (1989)].
3. Alanine-rich sequences are used to promote helix formation [S. Marqusee, V. H. Robbins, R. L. Baldwin, *Proc. Natl. Acad. Sci. U.S.A.* **86**, 5286 (1989)]. Synthesis of the peptides and coupling of the NTGs has been described elsewhere (*1*). 1,4-Methylaminobenzoic acid and terephthalic acid were purchased from Aldrich, and succinic acid-1,4-$^{13}C_2$ was purchased from Cambridge Isotope Laboratories. The identities of the peptides with NTGs attached were confirmed by mass spectrometry on a LASERMAT mass spectrometer (Finnegan MAT, Hemel Hempstead, United Kingdom) or by Mass-Search, Inc., Modesto, CA.
4. The values of $[\theta]_{222}$ (molar ellipticity at 222 nm) for peptide F_S with neutral MABA, TPA, and SUC attached (pH 7 for MABA and pH 1 for TPA and SUC) are −34,000, −34,000, and −36,000 ± 3000 degree cm^2 dmol^{-1}, respectively. $[\theta]_{222}$ for the peptides with NTGs attached was calculated on the basis of the concentration determined from quantitative amino acid analysis of solutions of known ellipticity. The peptide melting temperature (T_m in Table 1) is taken to be the temperature at which the derivative of the CD signal at 222 nm versus $1/T$(K) [where T(K) is the temperature in kelvin] is a minimum [C. R. Cantor and P. R. Schimmel, *Biophysical Chemistry* (Freeman, New York, 1980)]. For all of the helical peptides with NTGs attached, the thermal transitions are concentration-independent between 4 and 70 μM (up to 4 mM for peptide F_S with MABA). CD data were obtained in a 1-cm cell with an AVIV 62DS CD spectrometer (Aviv Associates, Lakewood, NJ) equipped with a thermoelectric temperature control unit.
5. The 2D ^{1}H NMR data were obtained on a Bruker AMX 500 MHz spectrometer (Bruker Instruments, Billerica, MA) at 3°C. The sample concentrations were typically 4 mM. Nuclear Overhauser and exchange spectroscopy (NOESY) data were obtained with a mixing time of 200 ms, and water was presaturated for 1.8 s. The data were processed and the crosspeaks integrated with the program FTNMR (Hare Research, Woodinville, WA). All spectra were processed with a 45° shifted sine bell window and a linear base line correction in both t_2 and t_1 (pulse time) dimensions. To reduce spectral overlap, we obtained the NOESY data for peptide F_S with MABA attached with a selectively deuterated version of the peptide in which the Ala β methyl groups are deuterated, except for Ala residues 1 to 4.
6. For peptide F_S with MABA and TPA attached, we observe (Table 2) strong sequential H^N_i–H^N_{i+1} NOE crosspeaks starting from the amide proton of residue 1, strong H^{α}_1–H^{β}_4 NOEs, and moderate H^{α}_1–H^N_4 NOEs, which suggests that the NH_2-termini of these helices are not frayed significantly (with SUC attached, some of these crosspeaks cannot be assigned unambiguously because of spectral overlap). A small degree of fraying, however, cannot be ruled out [A. Chakrabartty, J. A. Schellman, R. L. Baldwin, *Nature* **351**, 586 (1991); M. I. Liff *et al.*, *J. Am. Chem. Soc.* **113**, 1014 (1991); S. M. Miick *et al.*, *Biochemistry* **30**, 9498 (1991); C. A. Rohl *et al.*, *ibid.* **31**, 1263 (1992)]. Any fraying will tend to reduce the ΔpK_a values and increase the estimates of the dielectric screening effects. In an isolated α helix, the NOE between the α proton of residue i and the β protons of an Ala at position $i + 3$ is expected to be substantially more intense than the corresponding H^{α}_i–H^N_{i+3} NOE, whereas in a 3_{10} helix, the H^{α}_i–H^{β}_{i+3} and H^{α}_i–H^N_{i+3} NOEs are expected to be of similar intensity [K. Wüthrich, *NMR of Proteins and Nucleic Acids* (Wiley, New York, 1986)]. Thus, the NMR data are consistent with α-helical structure at the NH_2-terminus and not the 3_{10}-helical structure suggested from electron spin resonance and infrared absorption experiments on 16-residue, Ala-based peptides [S. M. Miick, G. V. Martinez, W. R. Fiori, A. P. Todd, G. L. Millhauser, *Nature* **359**, 653 (1992)].
7. The buffer for all optical experiments contained 1 mM sodium citrate, 1 mM sodium phosphate, and 1 mM sodium borate with no added salt unless specified. For all pK_a measurements, the pH of the sample was measured at room temperature after the determination of absorbance or chemical shift. The pK_a values were determined by a fit of the data to a single ionization equilibrium. Because the largest source of uncertainty is systematic error in the measurement of pH, the experiments were performed in parallel (folded and unfolded in pairs). This procedure reduces the uncertainty in the ΔpK_a values to less than the uncertainty in the absolute measure of any individual pK_a value.
8. The pK_a values for MABA and TPA attached to the peptides were determined from the pH dependence of a near-ultraviolet absorption band. For MABA, the maximum absorbance change occurs near 295 nm, and for TPA the maximum change is near 243 nm. The peptide concentration for optical experiments was typically 15 μM for MABA and 45 μM for TPA (a higher concentration was used for TPA because the magnitude of the absorbance change with pH is considerably smaller). The absorption data were recorded in a cell (1-cm path length) at 0°C on an Aviv Associates 118DS spectrophotometer.
9. We obtained the pK_a value of SUC attached to the peptides by monitoring the ^{13}C chemical shift of the SUC carboxyl carbon labeled specifically with ^{13}C. The ^{13}C NMR experiments were performed at 3°C in the same buffer used for the optical experiments at a peptide concentration between 1 and 3 mM. The succinyl methylene protons were decoupled during observation of the ^{13}C free induction decay (FID) with a WALTZ-16 decoupling scheme [A. J. Shaka, J. Keeler, R. Freeman, *J. Magn. Reson.* **53**, 313 (1983)].
10. P. G. Thomas, A. J. Russell, A. R. Fersht, *Nature* **318**, 375 (1985).
11. K. R. Shoemaker, P. S. Kim, E. J. York, J. M. Stewart, R. L. Baldwin, *ibid.* **326**, 563 (1987).
12. T. Takahashi, H. Nakamura, A. Wada, *Biopolymers* **32**, 897 (1992).
13. J. G. Kirkwood and F. H. Westheimer, *J. Chem. Phys.* **6**, 506 (1938).
14. J. Sancho, L. Serrano, A. R. Fersht, *Biochemistry* **31**, 2253 (1992).
15. W. G. J. Hol, P. T. van Duijnen, H. J. C. Berendsen, *Nature* **273**, 443 (1978); W. G. J. Hol, L. M. Halie, C. Sander, *ibid.* **294**, 532 (1981); H. Nicholson, W. J. Becktel, B. W. Matthews, *ibid.* **336**, 651 (1988); D. Šali, M. Bycroft, A. R. Fersht, *ibid.* **335**, 740 (1988); L. Serrano and A. R. Fersht, *ibid.* **342**, 296 (1989); R. Fairman, K. R. Shoemaker, E. J. York, J. M. Stewart, R. L. Baldwin, *Proteins* **5**, 1 (1989); H. Nicholson, D. E. Anderson, S. Dao-pin, B. W. Matthews, *Biochemistry* **30**, 9816 (1991).
16. Long helices are not required for significant interactions with the backbone because electrostatic interactions decrease rapidly with distance and are dominated by the closest groups. For a dipole located at the center of MABA, it is estimated from simple electrostatics [as in (*18*)] that ~80% of the backbone-dipole interaction energy is from residues in the first helical turn (first four amide groups), and ~90% of the total is from residues in the first two turns (first seven amide groups). For the charges on MABA and TPA, we estimate that the first two turns account for ~75%, and for SUC the first two turns account for ~85% of the total interaction. These estimates are consistent with the calculations in (*17*).
17. J. Åqvist, H. Luecke, F. A. Quiocho, A. Warshel, *Proc. Natl. Acad. Sci. U.S.A.* **88**, 2026 (1991).
18. To estimate the interaction energy between the NH_2-terminal charges and the helix backbone in the absence of an environment, we built a 21-residue Ala α helix (backbone dihedral angles φ and ψ set to −63° and −41°, respectively) with bond lengths, bond angles, and partial charges assigned by the CHARMM [B. R. Brooks *et al.*, *J. Comput. Chem.* **4**, 187 (1983)] parameter sets (PARAM19 and TOPH19). An interaction energy was calculated with Coulomb's law and a dielectric constant of 1. For MABA and TPA, the charge was assumed to be located 6 Å from the carbonyl carbon of the amide bond between the peptide

and the NTGs, in the direction of the C–C bond between the carbonyl carbon and the aromatic ring. The position of the carbonyl carbon is defined by the angle ϕ (−63°) and is consistent with α-helical structure at the NH_2-terminus and a hydrogen bond between the probe carbonyl oxygen and the amide NH of residue 4 (*1*). The charge on SUC is placed 3.5 Å from the amide nitrogen atom of residue 3 in the direction of the N–H bond. The calculated backbone-charge interaction energy for a 41-residue Ala α helix is larger than for the 21-residue helix by ~11% for the charge position assumed for MABA and TPA and by ~5% for SUC.

19. C. Tanford and J. G. Kirkwood, *J. Am. Chem. Soc.* **79**, 5333 (1957); D. C. Rees, *J. Mol. Biol.* **141**, 323 (1980); J. A. Wells, D. B. Powers, R. R. Bott, T. P. Graycar, D. A. Estell, *Proc. Natl. Acad. Sci. U.S.A.* **84**, 1219 (1987).
20. M. K. Gilson, A. Rashin, R. Fine, B. Honig, *J. Mol. Biol.* **183**, 503 (1985).
21. The negative charge on the deprotonated SUC group interacts favorably with the helical backbone, and this may result in restriction of rotation about some of the succinyl C–C single bonds. Restricted motion is suggested by an increase in the intensity of NOEs between the SUC methylene protons and the β protons of residue 3 when the group is negatively charged (D. J. Lockhart and P. S. Kim, unpublished results). Because of this possible entropic contribution, the measured value of $\Delta\Delta G_F$ for SUC is a lower limit for the strength of the purely electrostatic interaction between the negative charge and the backbone, and the ε_{eff} value of 95 is an upper limit.
22. Neutral MABA is somewhat dipolar, and the dipole moment is approximately aligned with the electric field produced by the helix (*1*). Protonated MABA, however, is expected to be less dipolar because of the reduced importance of charge-separated resonance forms. Thus, there is an additional unfavorable electronic contribution to the free energy of protonation of MABA in the presence of helical structure, and the ε_{eff} value of 40 calculated from the MABA pK_a shift data is a lower limit. Given a physically reasonable upper limit of ~100, the ε_{eff} values obtained from the ΔpK_a data for all three titratable probe groups are qualitatively consistent.
23. F. H. Westheimer and J. G. Kirkwood, *J. Chem. Phys.* **6**, 513 (1938).
24. F. W. Baker, R. C. Parish, L. M. Stock, *J. Am. Chem. Soc.* **89**, 5677 (1967).
25. Measurements on benzyl aspartate polymers (with polar groups at the para position of the benzyl group) suggest that interactions between dipolar side chains and the helix backbone can be significant in determining the helical sense of the polymer [A. Wada, *Adv. Biophys.* **9**, 1 (1976)]. The stability of a neutral helix has been observed to increase linearly with ionic strength [J. M. Scholtz *et al.*, *J. Am. Chem. Soc.* **113**, 5102 (1991)].
26. J. G. Kirkwood, *J. Chem. Phys.* **2**, 351 (1934); T. L. Hill, *J. Phys. Chem.* **60**, 253 (1956); S. Ehrenson, *J. Am. Chem. Soc.* **98**, 7510 (1976); J. Warwicker and H. C. Watson, *J. Mol. Biol.* **157**, 671 (1982); D. Bashford and M. Karplus, *Biochemistry* **29**, 10219 (1990).
27. For a point dipole, the electric field is inversely proportional to the distance cubed and the electrostatic potential is inversely proportional to the distance squared. For a charge, the electric field is inversely proportional to distance squared and the potential is inversely proportional to distance to the first power.
28. We note that the center of the dipolar charge distribution for the neutral dipolar probe (MABA) used previously (*1*) is not located at exactly the same position as the center of the charges on MABA and TPA. Although it is difficult to evaluate the effect of this difference, it is not expected to be a dominant factor in determining differential screening effects because both the charged and dipolar groups used here are highly accessible to solvent.
29. T. Sakamoto, H. Nakamura, H. Uedaira, A. Wada, *J. Phys. Chem.* **93**, 357 (1989).
30. Y.-H. Chen, J. T. Yang, K. H. Chau, *Biochemistry* **13**, 3350 (1974).
31. We thank R. Rutkowski, M. Milhollen, and M. Burgess for peptide synthesis, attachment of the probes, and mass spectrometry; S. Stradley for amino acid analysis; Z. Peng and L. McIntosh for help with NMR; B. Tidor for help with CHARMM; and B. Tidor, Z. Peng, J. Weissman, and P. Petillo for helpful discussions. D.J.L. is supported by a Damon Runyon–Walter Winchell Cancer Research Fund Fellowship. P.S.K. is a Pew Scholar in the Biomedical Sciences. Supported by the Howard Hughes Medical Institute.

6 November 1992; accepted 28 January 1993

Pressure-Induced Amorphization of *R*-Al_5Li_3Cu: A Structural Relation Among Amorphous Metals, Quasi-Crystals, and Curved Space

Robert R. Winters and William S. Hammack*

A central question in the study of amorphous materials is the extent to which they are ordered. When the crystalline intermetallic *R*-Al_5Li_3Cu is compressed to 23.2 gigapascals at ambient temperature, an amorphous phase is produced whose order can be described as defects in a curved-space crystal. This result supports a structural relation between quasi-crystals and amorphous metals based on icosahedral ordering. This result also shows that a metallic crystal can be made amorphous by compression.

A central question in the study of amorphous materials is: "How disordered are they?" (*1*). Formally this is known as the problem of medium-range order (MRO), that is, order on the length scale 5 to 20 Å. Experimentally MRO is difficult to measure, although recent work has shown conclusively ordering to ~10 Å for an alkali silicate glass (*2*). Also, the phenomenon of pressure-induced amorphization, a new method for preparing amorphous solids at ambient temperature by compression, has demonstrated a sense of order in amorphous solids (*3–9*). The difficult aspect is how to describe this "new" order in amorphous materials. The most common approach is to establish the short-range order in the amorphous material and then look for the topological rules that govern the MRO (*10*).

Several researchers have proposed that the order in amorphous metals can be found by examining a perfect crystal formed in a curved space (*11, 12*). Sadoc and Rivier showed how decurving this perfect crystal can produce a metal alloy or an amorphous metallic structure (*13*). Similarly, Nelson used the perfect curved-space crystal to define defects in icosahedral bond orientational order (*11*). The major point of their work was to change the level at which disorder is considered. Rather than focusing on the irregular arrangement of atoms, one focuses on the structure of the defects because they are defined relative to a perfect state in curved space.

In this work we show that compression can produce an amorphous metallic alloy whose order is described in curved space. Moreover, this result shows that we have observed the pressure-induced amorphization of a crystalline metal. The preparatory method is also unusual because the amorphous solid is produced without quenching: typically ultrahigh quench rates, on the order of 10^6 °C/s, are needed to produce amorphous metals (*10*).

To understand the curved-space ideas mentioned above, we must review several packing principles of metallic alloys. Metallic alloys prefer to have a coordination shell of 12 atoms in the shape of an icosahedron (*14, 15*). This arrangement allows the densest local packing and hence the lowest energy (*16*). A crystal consisting of only perfect icosahedral coordination shells is incompatible with space-filling requirements; this balance between locally low-energy noncrystallographic packings and long-range periodicity has been called "topological frustration" (*8, 17*). Nature adjusts this frustration by mixing different coordination shells—coordinations of 14, 15, or 16 atoms—forming what are called Frank-Kasper phases (*18, 19*). These alloys are composed of atoms of different sizes. Thus, purely tetrahedral packing is allowed, which results in a more efficient packing than cubic or hexagonal close packing. Because the Frank-Kasper phases have only slightly distorted tetrahedral interstices, they are often called tetrahedrally close-packed (tcp) structures (*14*).

A structure does exist in a curved space, however, in which every atom has perfect icosahedral coordination; it is called polytope {3,3,5}. It can be regarded as a four-dimensional analog of the regular icosahe-

Department of Chemical Engineering, Carnegie Mellon University, Pittsburgh, PA 15213.

*To whom correspondence should be addressed.